Supplementary Fig. 1

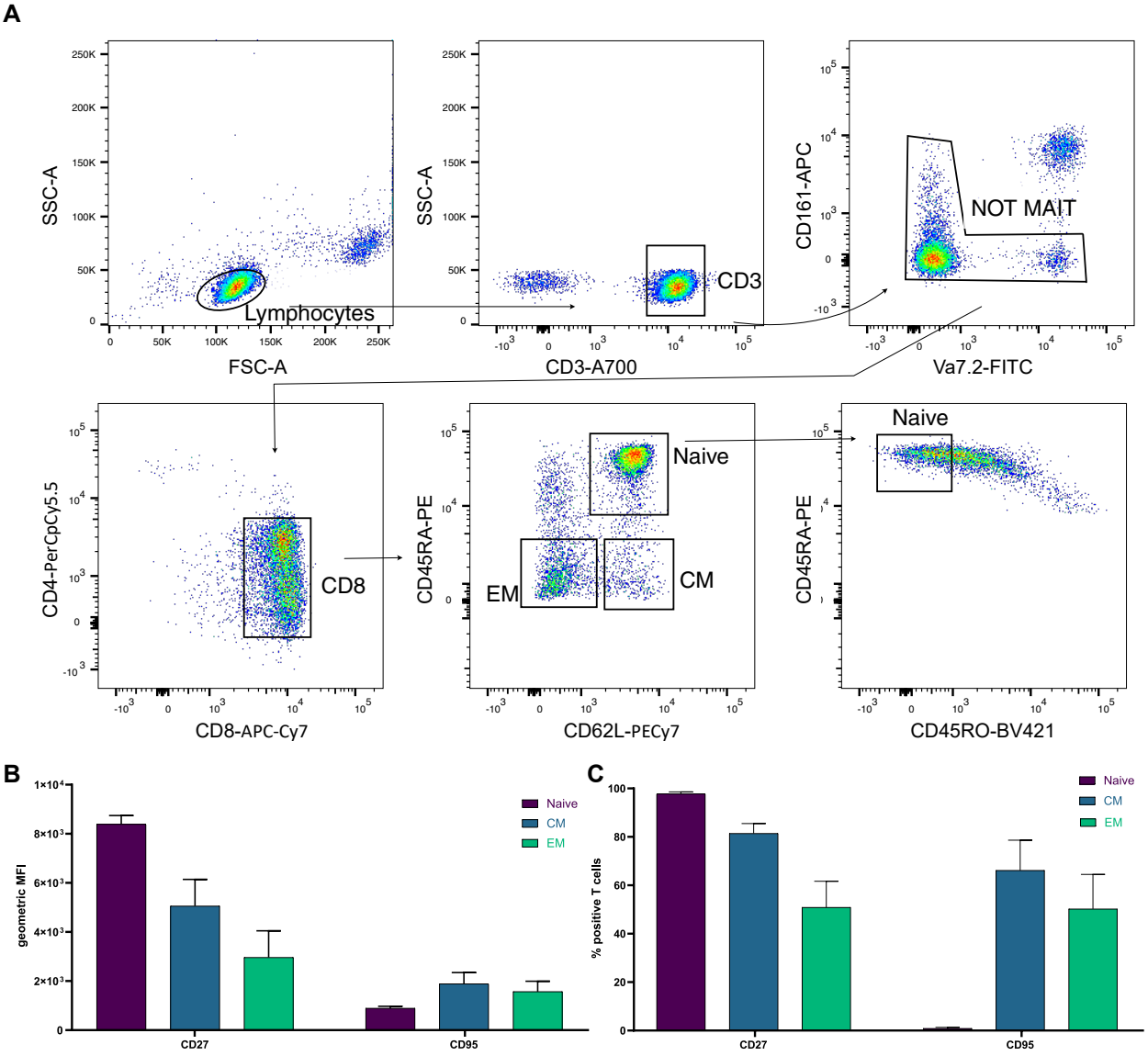

Supplementary Fig. 1. A. Sorting strategy for isolation of naïve (N), central memory (CM) and effector memory (EM) from human healthy donor (HD, n=6) CD8+ T cells following CD8+ T cell enrichment by negative selection from peripheral blood mononuclear cells (PBMCs). **B-C.** Mean expression + SD of memory associated markers in post-sorted CD8+ T cells by flow cytometry.

Supplementary Fig. 2

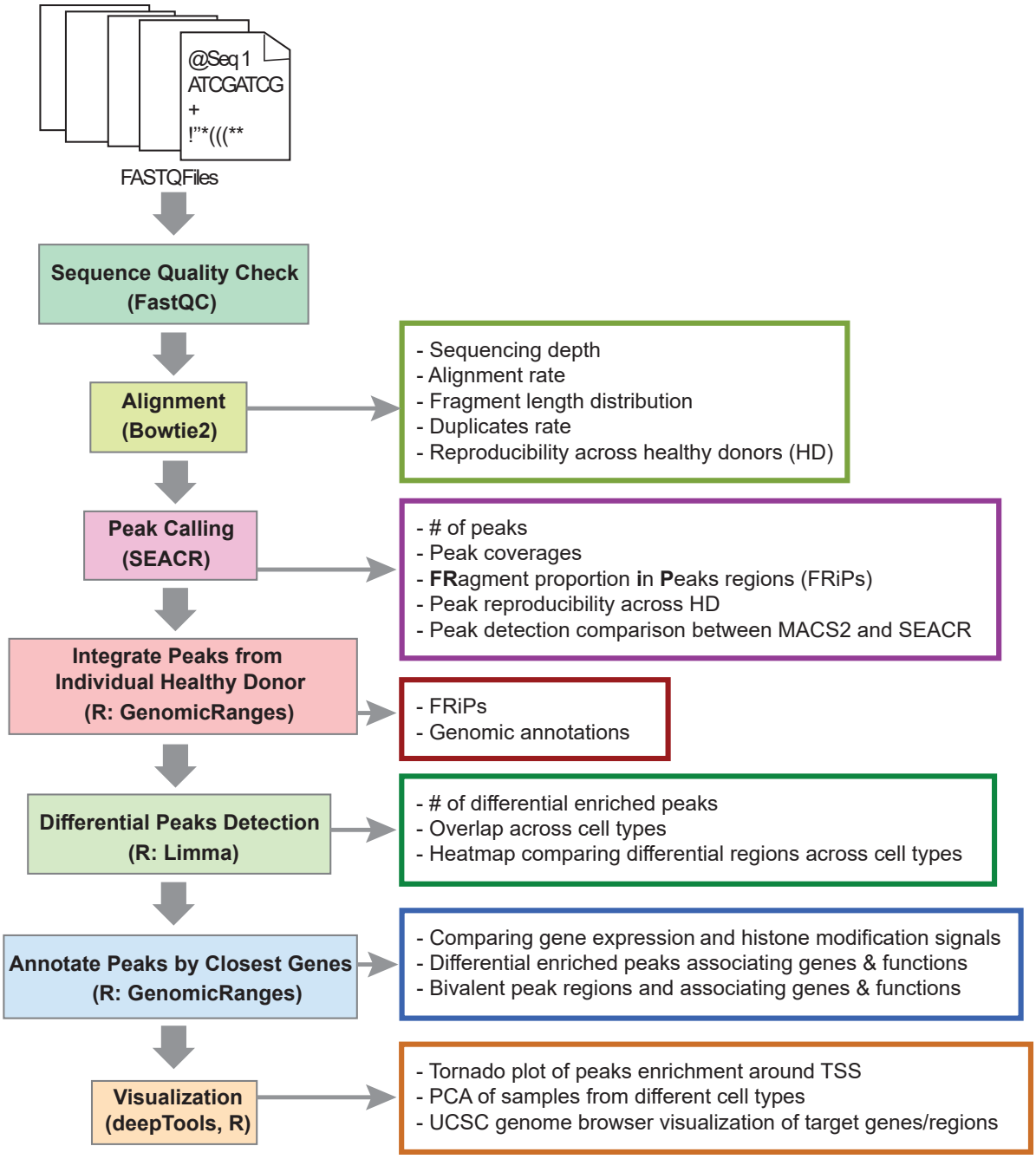

Supplementary Fig. 2. Bioinformatic workflow for analysis of CUT&RUN data.

Supplementary Fig. 3

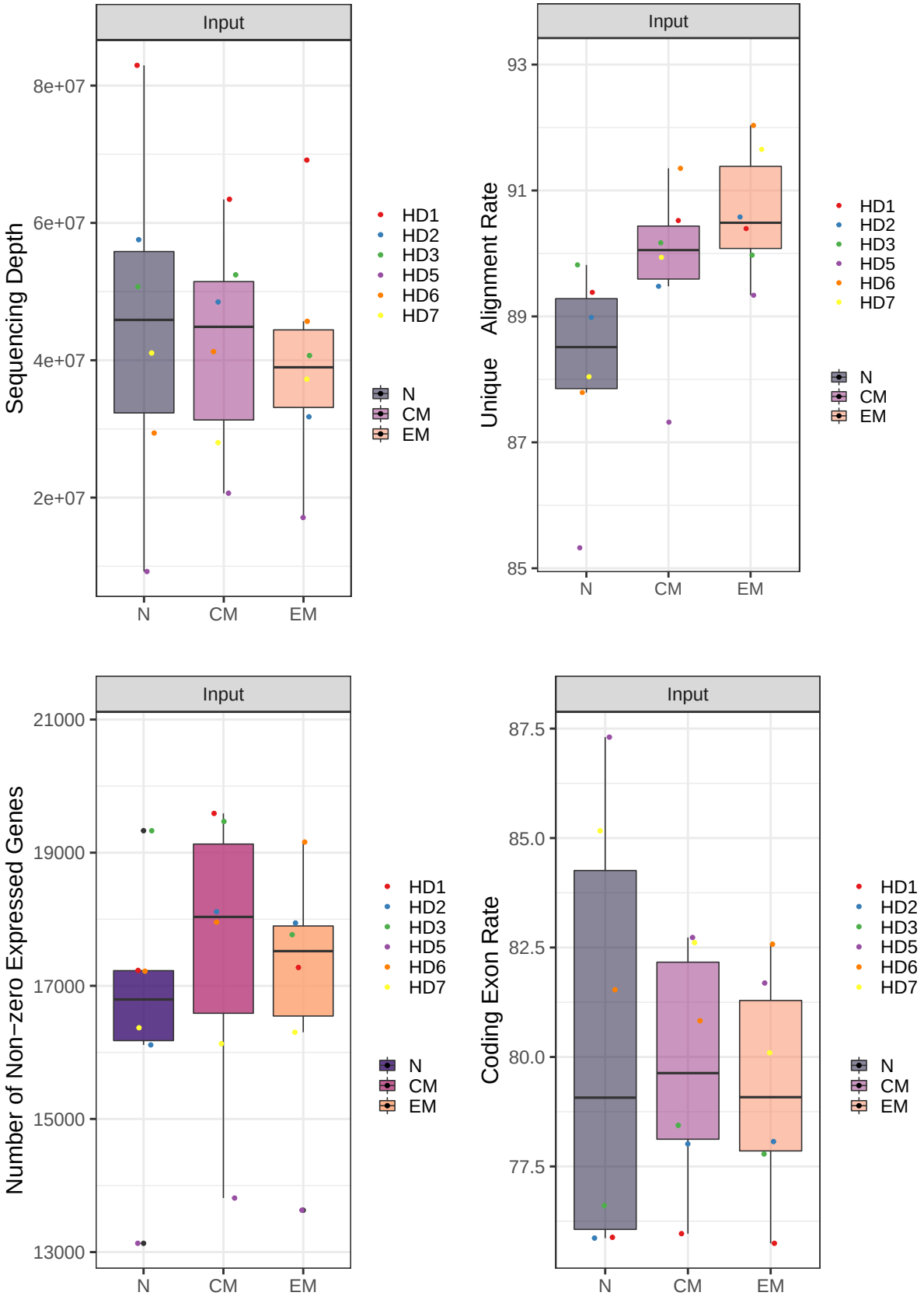

Supplementary Fig. 3. RNA-seq quality control metrics (mean +/- 95% consfidence interval and range). **A**. Sequencing depth **B**. Unique alignment rate (%), **C**. mappable number of non-zero expressed genes **D**. Coding exon rate (%). Line represents median, box represents inter

Supplementary Fig. 4

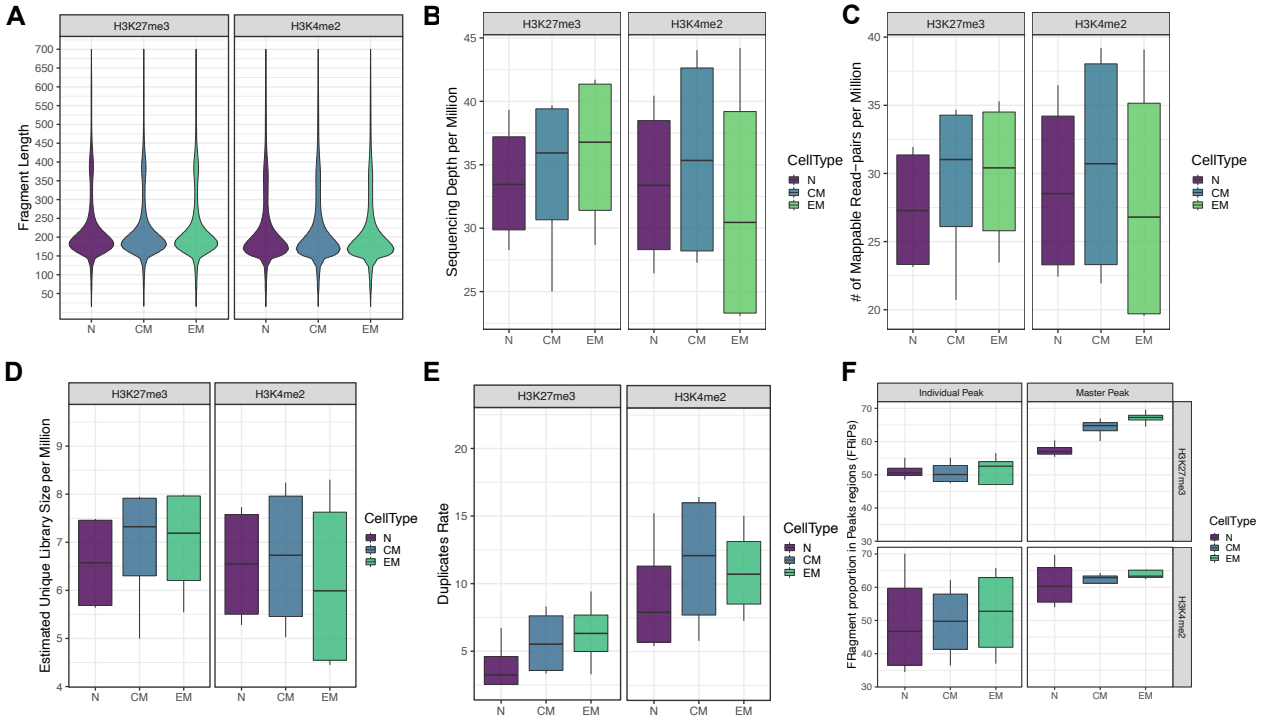

Supplementary Fig. 4. CUT&RUN quality control metrics**. A**. Fragment length (violin plot represents distribution with ranges), **B**. Mean sequencing depth, **C**. Mappable reads and **D**. Estimated unique library size +/- 95% confidence interval with range. **E**. Mean uplicate rate +/- 95% confidence interval with range. **F**. Mean fragment proportion in peak regions (FRIPs) in final master peak list +/- 95% confidence interval with range. Data represents intersection of top 10% of called peaks that are detected above IgG control. All QC metrics were consistent with previous CUT&RUN publications and is indicative of recurrent cut sites by endonuclease. Duplicates were retained as recommended for a high complexity library (D, Zhu, Orkin, Yuan *Genome Biology,* 2019).

Supplementary Fig. 5

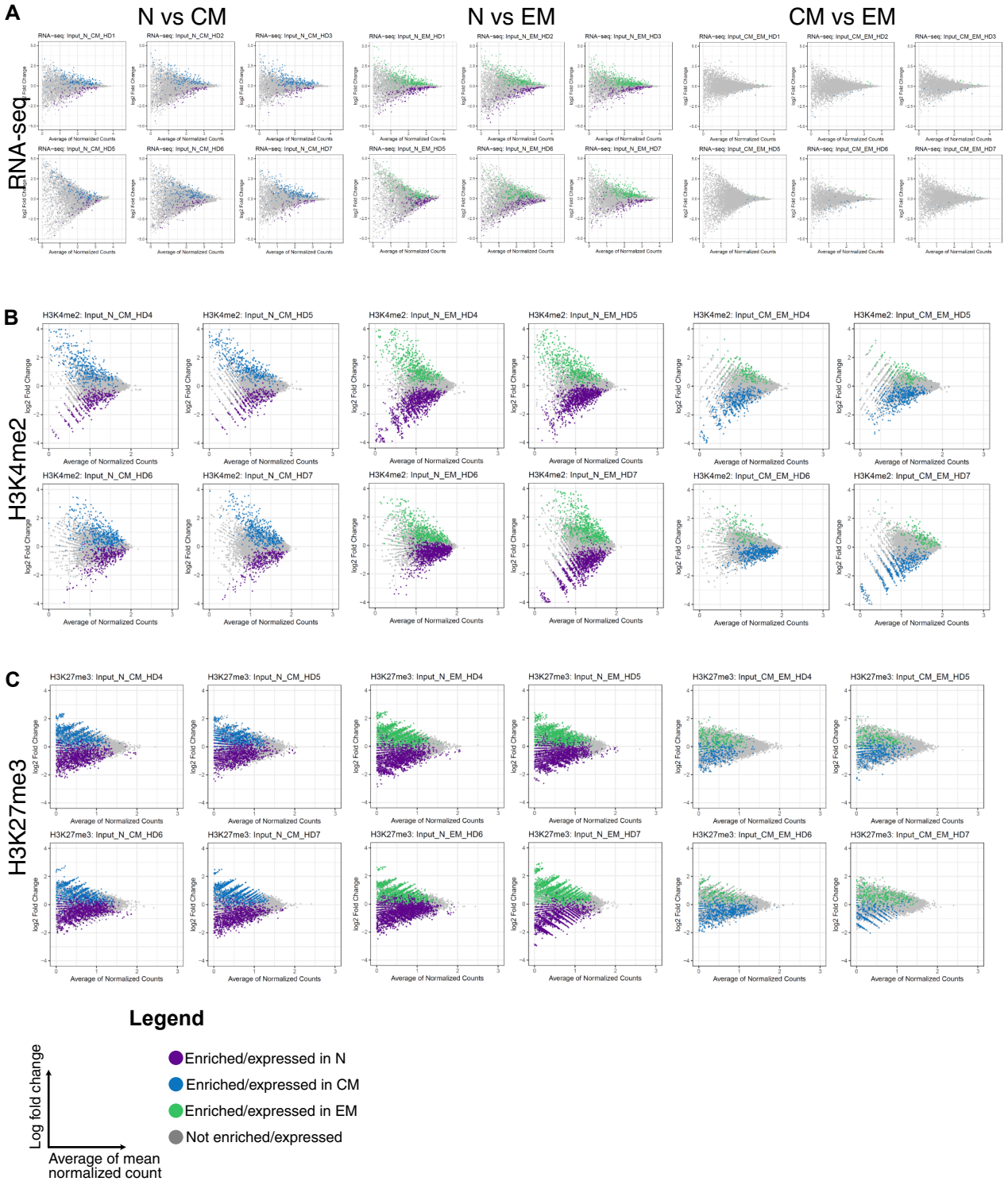

Supplementary Fig. 5. MA PLOT of **A.** RNA-seq, **B.** H3K4me2, and **c.** H3K27me3 data illustrating the distribution of log fold change in gene expression (or gene enrichment) relative to average of mean normalized signal per gene across individual donors. Each point represents an individual annotated gene.

Supplementary Fig. 6

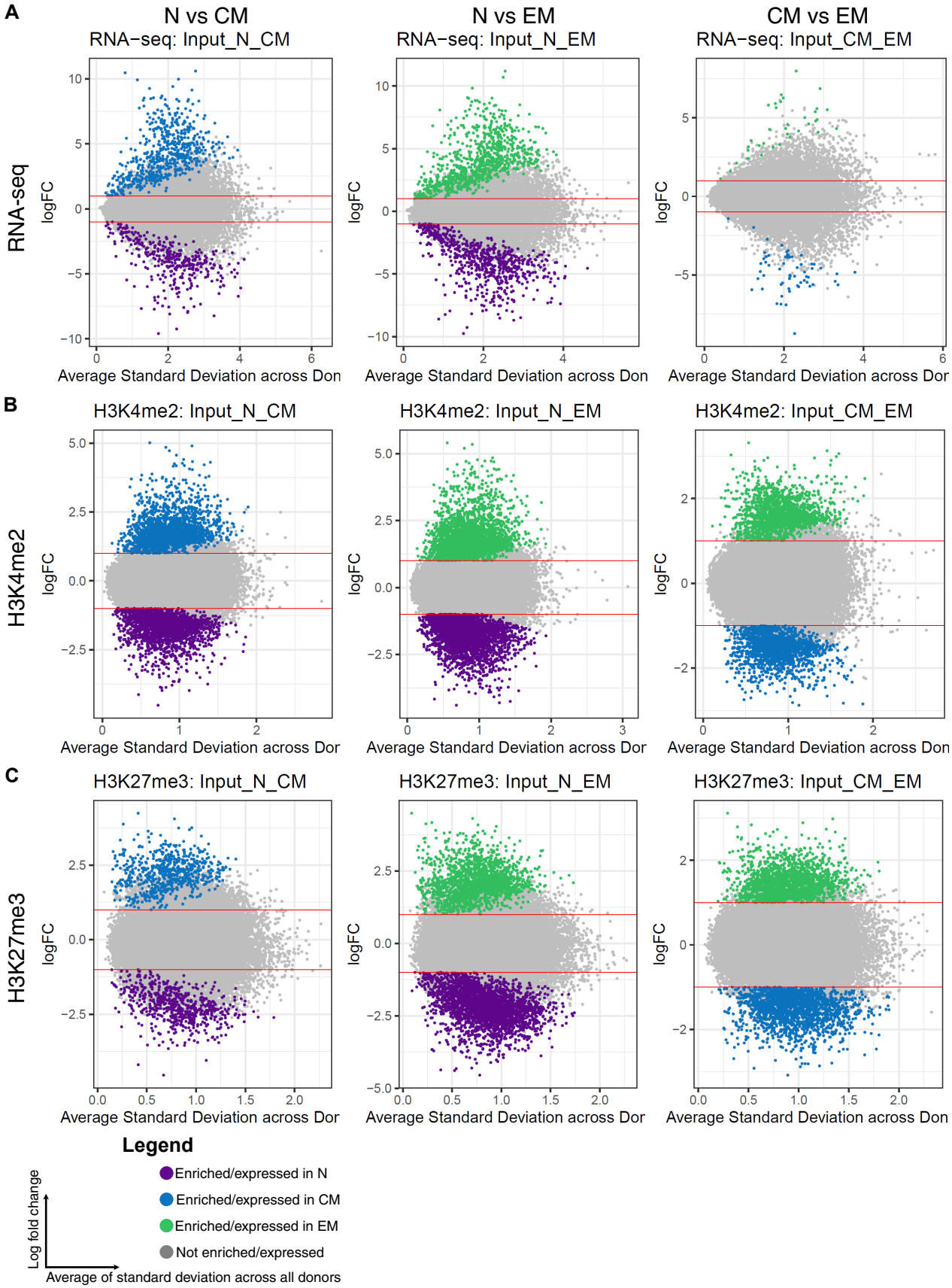

Supplementary Fig. 6. Log fold change analysis with respect to donor replicate variation **A.** RNA-seq, **B.** H3K4me2, and **c.** H3K27me3 data representing the average across donors for each gene. Each point

Supplementary Fig. 7

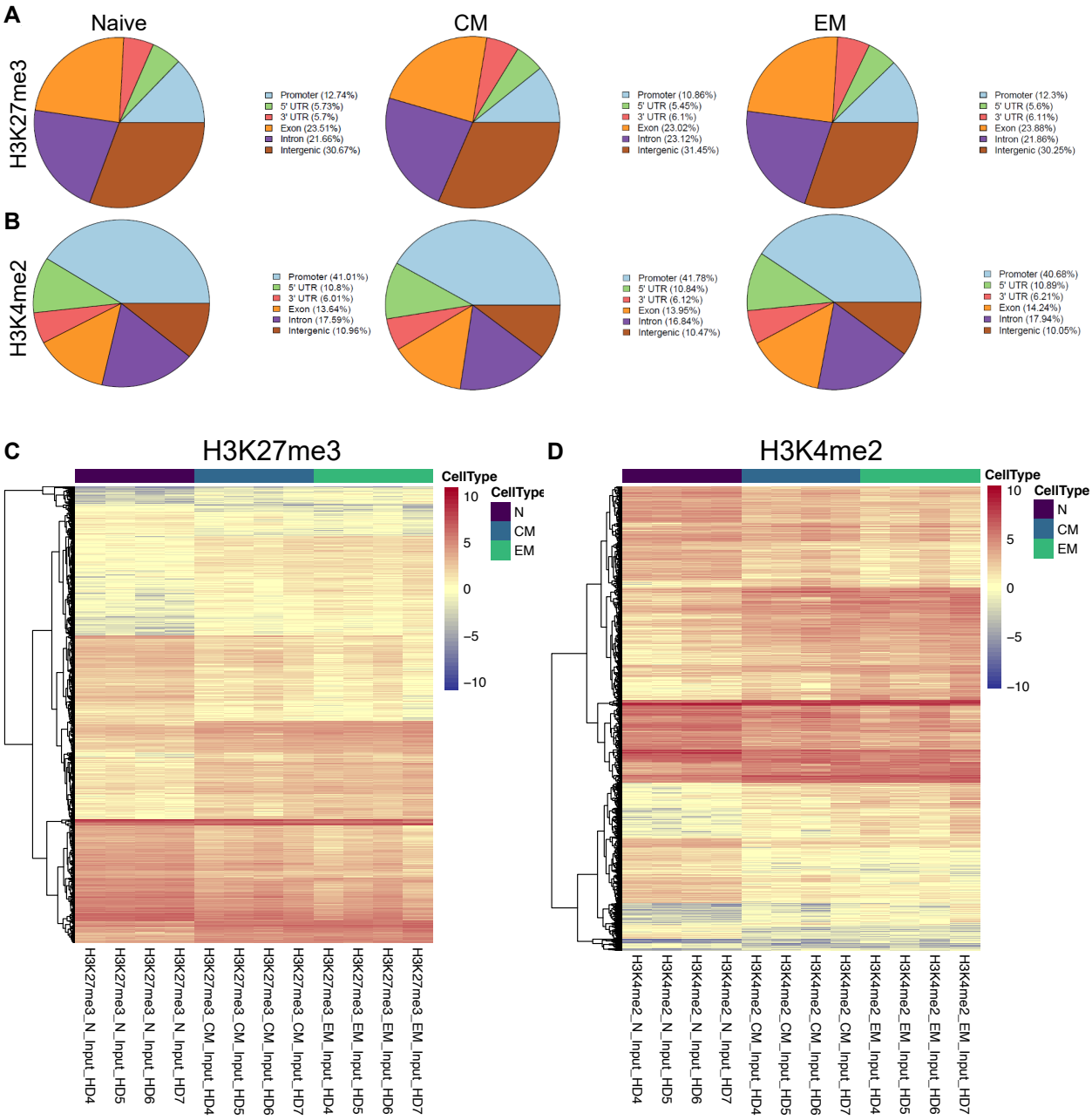

Supplementary Fig. 7. A. H3K27me3 genomic regions in T cell subsets. **B**. H3K4me2 genomic regions in T cell subsets. **C-D**. Heatmap of H3K27me3 (**C**) and H3K24me2 (**D**) reads across the genome from four donor T cell subsets with unsupervised clustering.

Supplementary Fig. 8

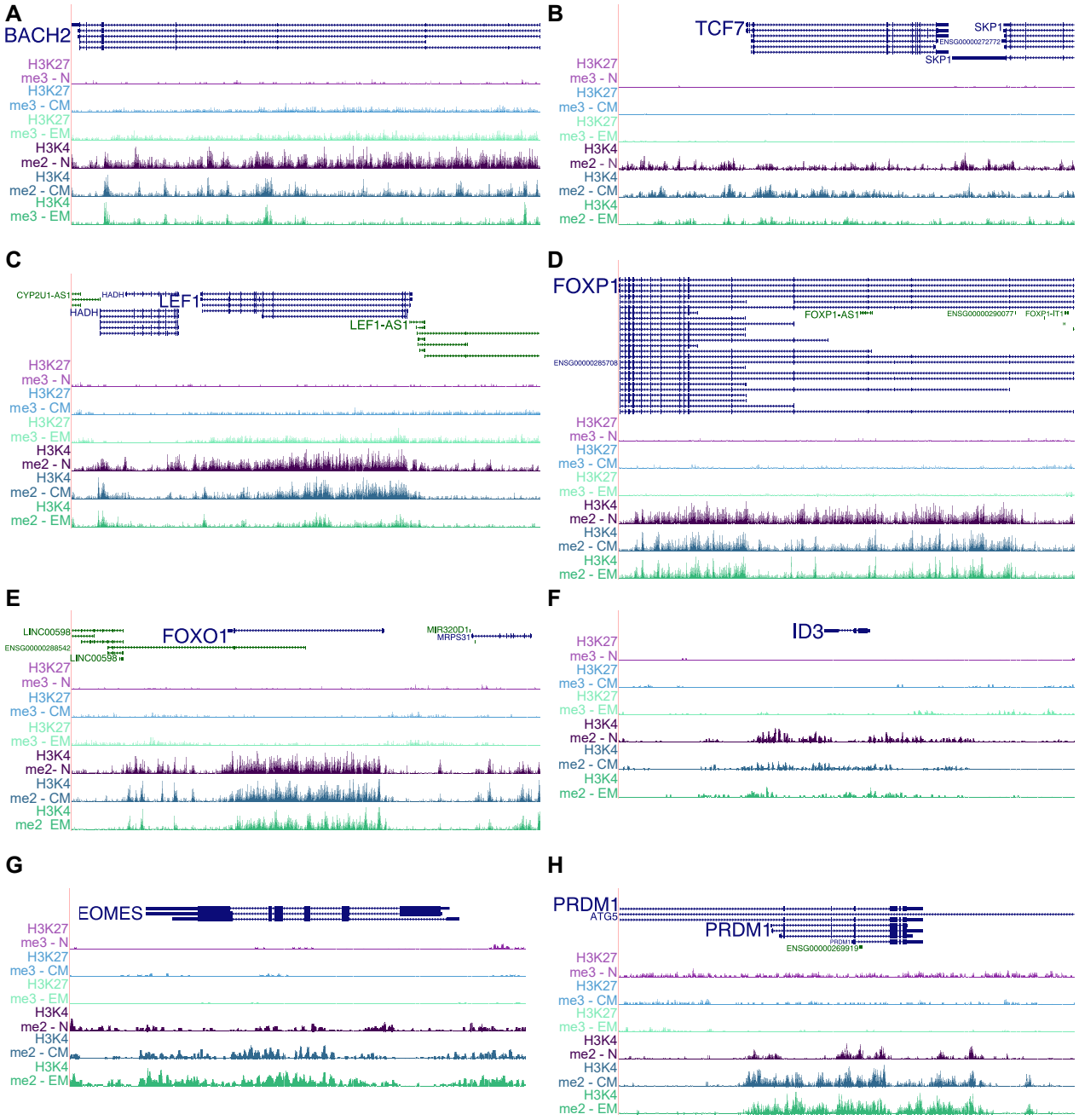

Supplementary Fig. 8. A-H. UCSC genome browser tracks comparing H4K2me2 and H3K27me3 marks for genes with known associations with CD8+ T cell memory formation and maintenance (**A-F**) and T cell exhaustion (**G-H**).

Supplementary Fig. 9

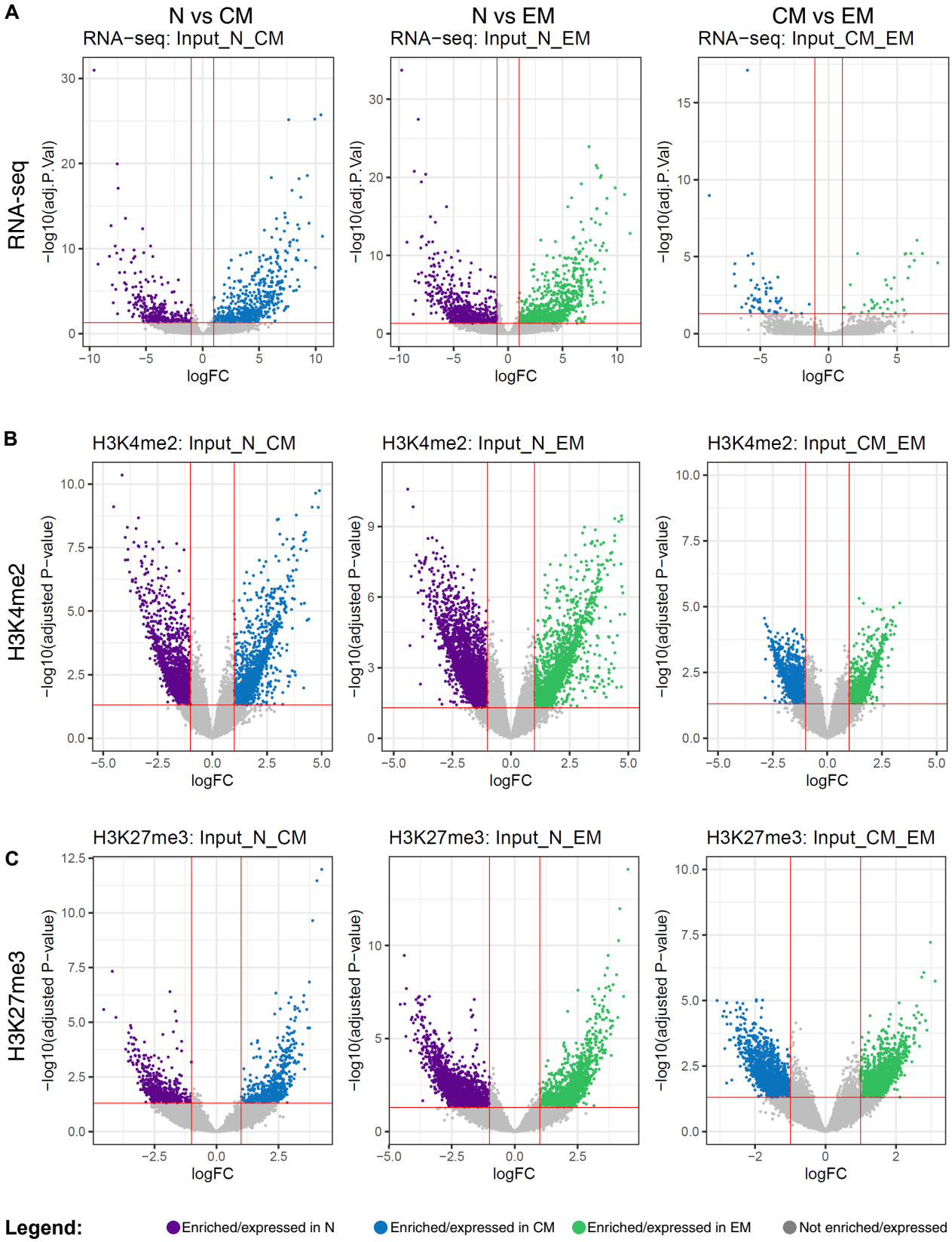

Supplementary Fig. 9. Volcano plot comparing N, CM and EM sorted subsets analyzed by **A.** RNA-seq, **B.** H3K4me2 and **C.** H3K27me3 enriched histone methylation marks. Adjusted P value by Benjamini-Hochberg

Supplementary Fig. 10

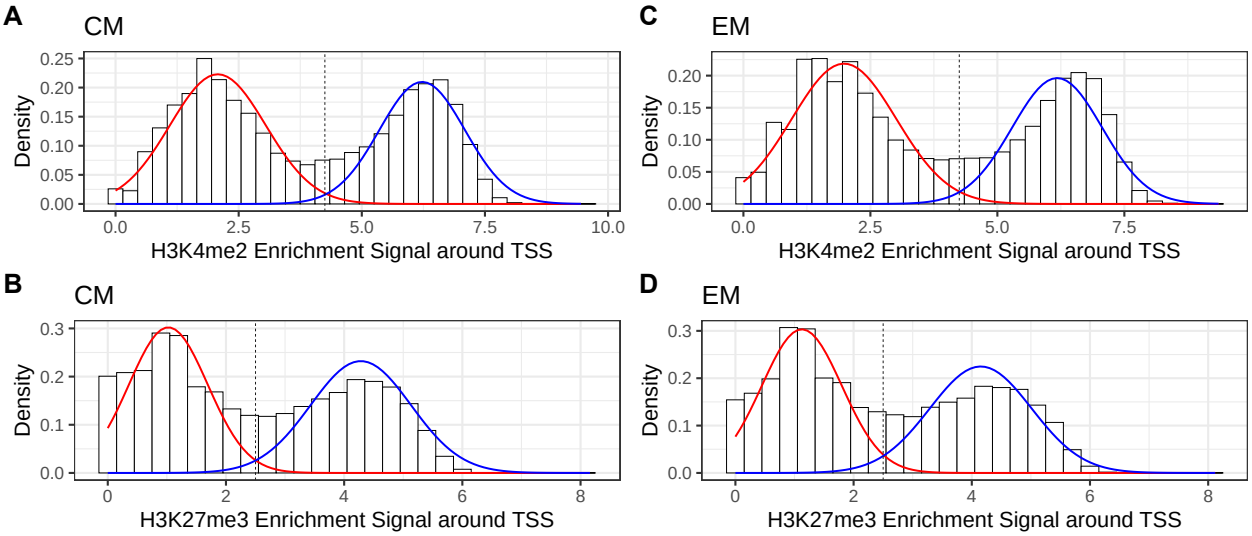

Supplementary Fig. 10. A-D. Gaussian mixture model of negative (red line) and positive (blue line) H3K27me3 and H3K4me2 reads in central memory (CM) and effector memory (CM) cells. Dashed line represents cut-off between positive and negative reads.

Supplementary Fig. 11

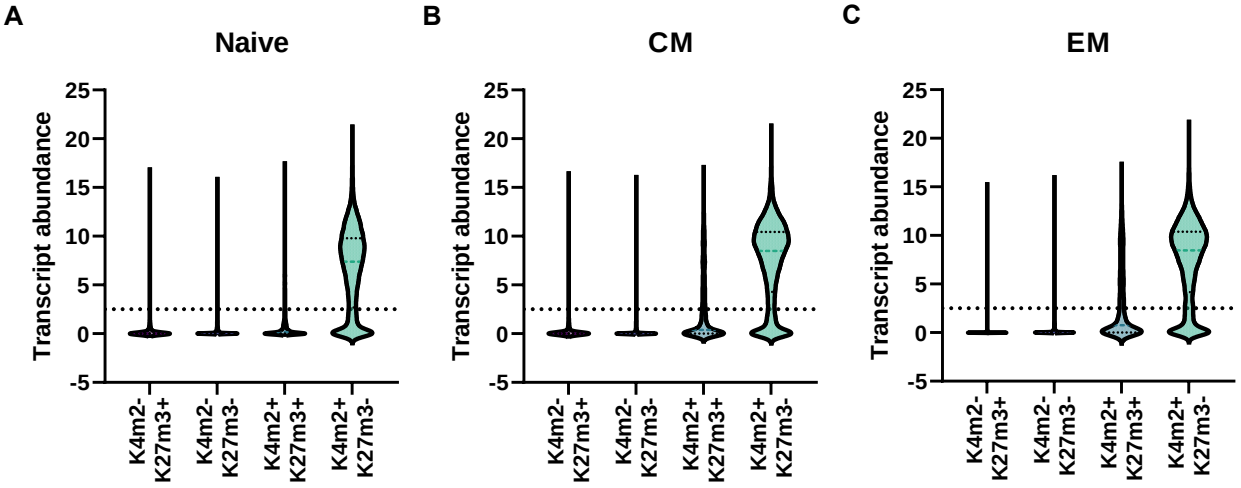

Supplementary Fig. 11. Absolute total transcript level with dotted line representing cut-off for high (RNA^{hi}) and low (RNA^{lo}) transcripts abundance. Violin plot represents data distribution with mean and 95% confidence interval and ranges.

Supplementary Fig. 12

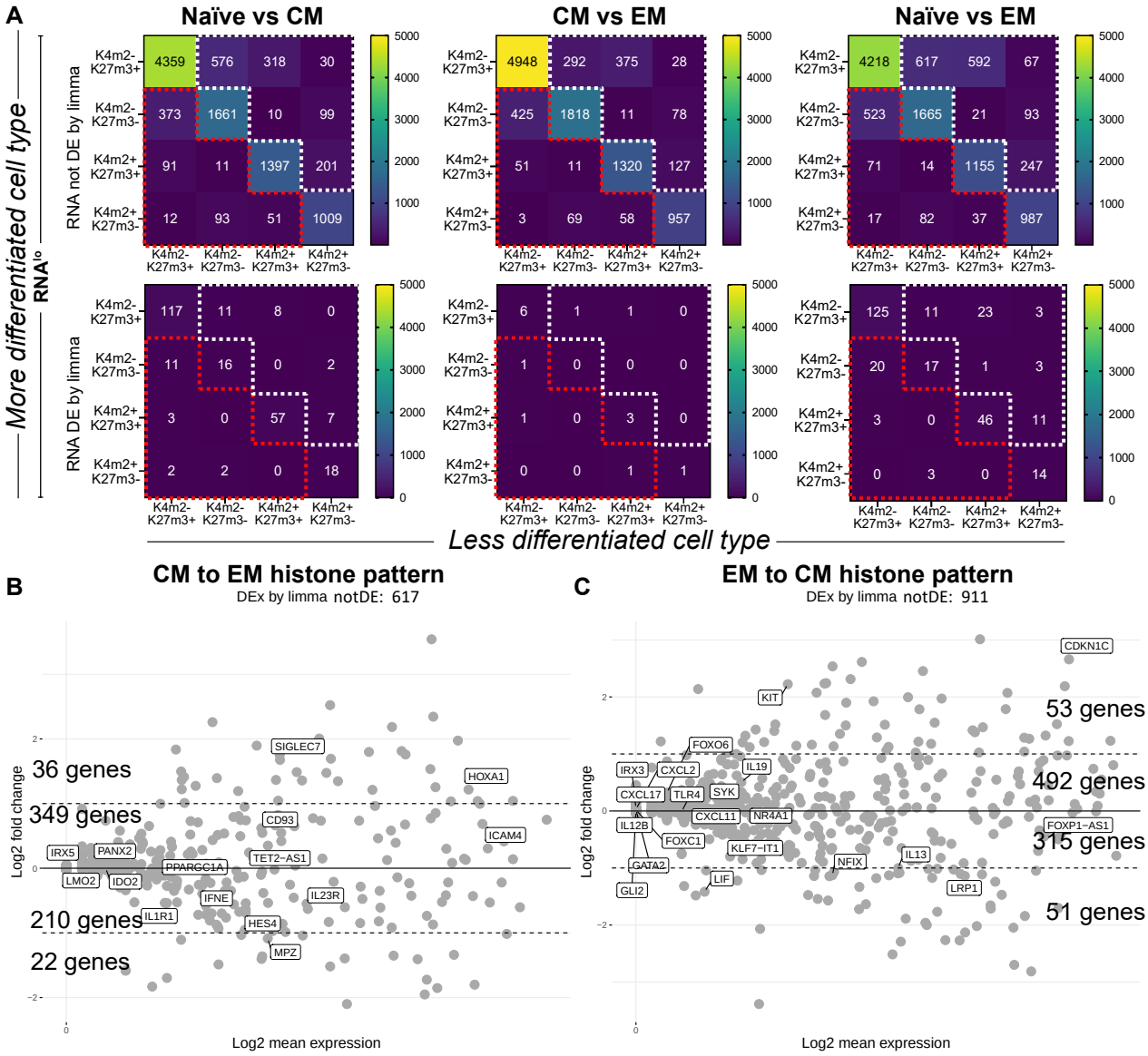

Supplementary Fig. 12. A. Histone mark patterns in RNA^{lo} genes when comparing ex vivo sorted CD8+ T cell subsets. **B**. Genes that show histone mark patterns indicative of EM cells when compared to CM cells (red box middle panel in A). **C**. Genes that show histone mark patterns indicative of CM cells when compared to EM cells (white box middle panel in A).

Supplementary Fig. 13

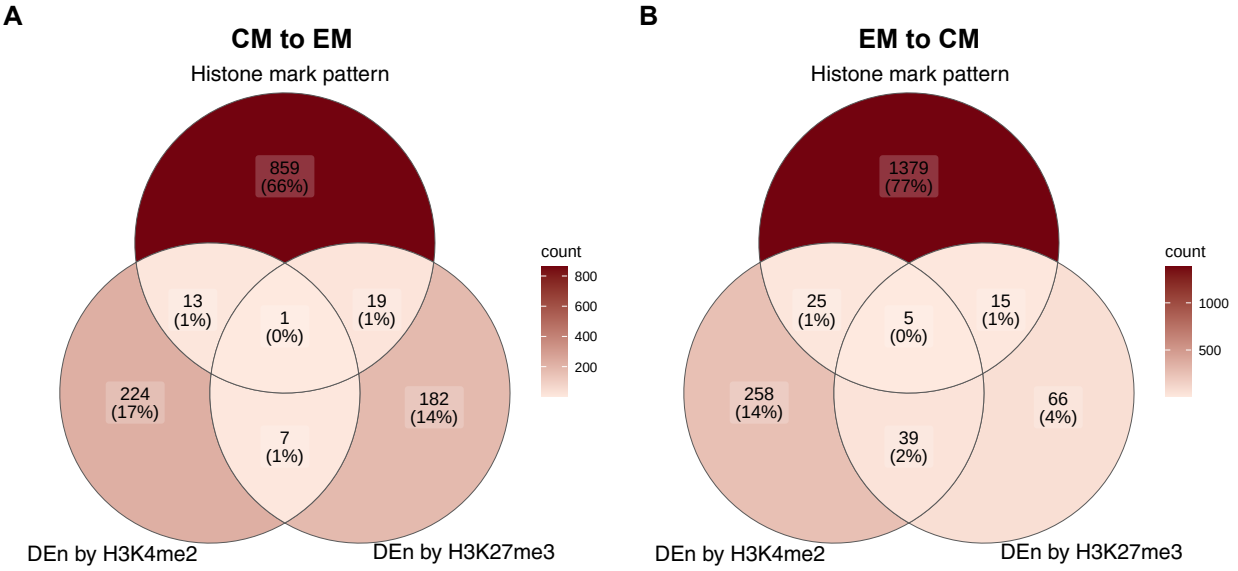

Supplementary Fig. 13. A. Comparison of number of genes that are biased towards EM subsets revealed by change in histone mark pattern versus changes in single H3K4me2 or H3K27me3 marks as analyzed by limma with logFC $\geq$ 1 and adjusted P value < 0.05. **B.** Comparison of number of genes that are biased towards CM subsets revealed by change in histone mark pattern versus changes in single H3K4me2 or H3K27me3 marks as analyzed by limma with logFC $\geq$ 1 and adjusted P value < 0.05.

Supplementary Fig. 14

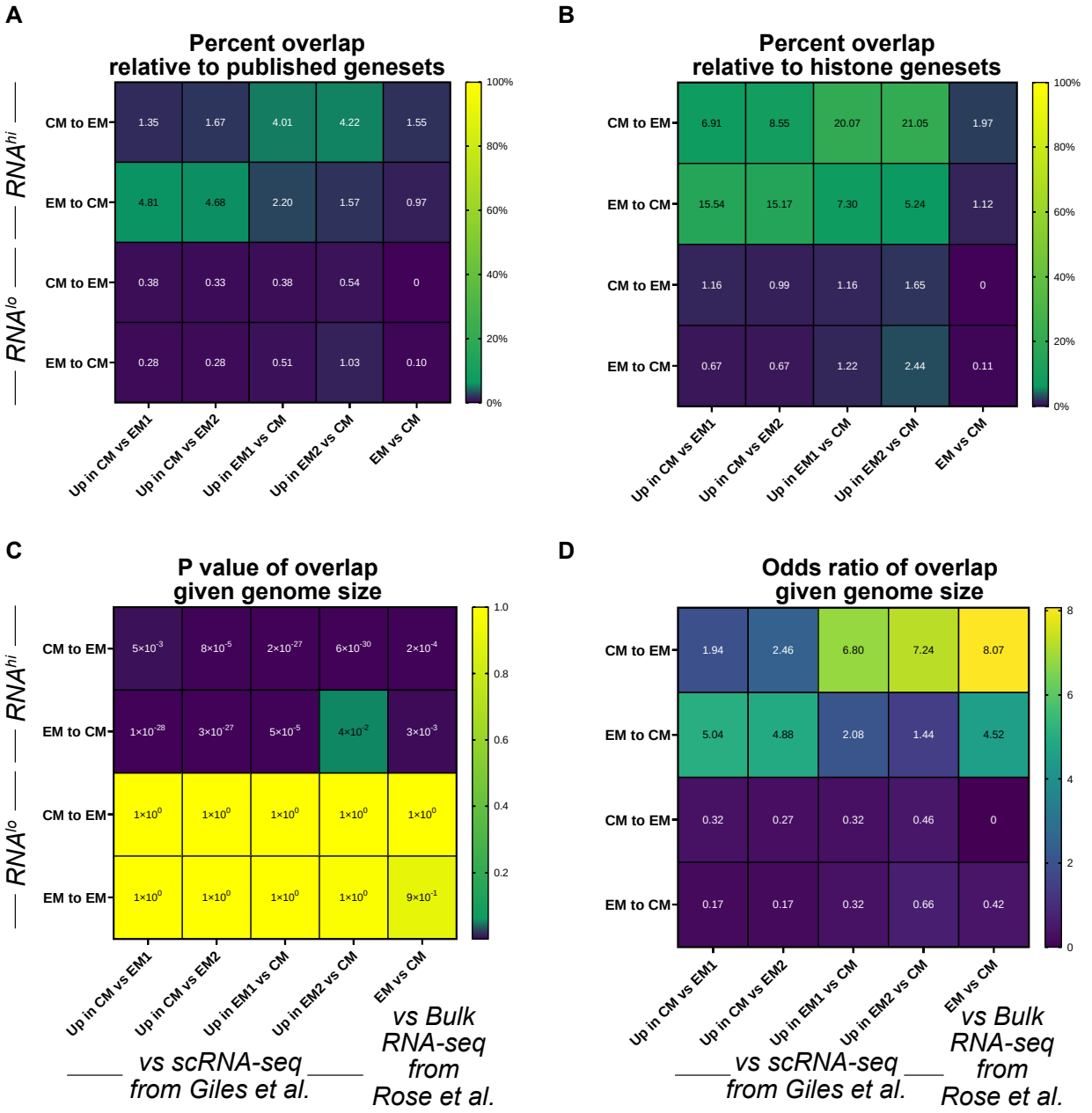

Supplementary Fig. 14. A-D. Statistics from GeneOverlap (Percent overlap, **A**; percent overlap of genes that change in histone mark divided published gene sets, **B**; P value of overlap, **C**; odds ratio of overlap, **D**) comparing genes with histone mark patterns indicative of EM cells (CM to EM) or CM cells (EM to CM) with published analyses comparing EM and CM cells by single cell (sc) RNA-seq or bulk RNA-seq. As per Giles et al. (2022), EM1 represent cells with EM immunophenotype and CD27+, and EM2 represent cells with EM immunophenotype and CD27-. P value by Fisher exact test.

Supplementary Fig. 15

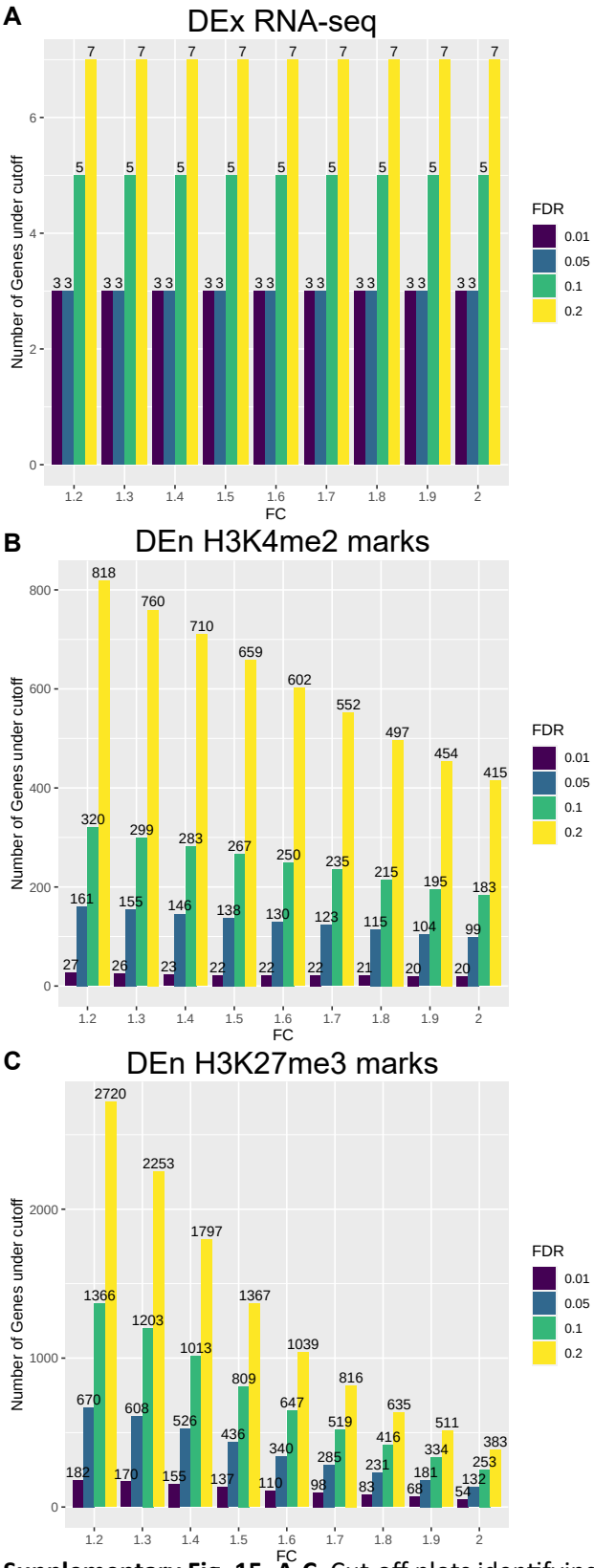

Supplementary Fig. 15. A-C. Cut-off plots identifying number of DEx by RNA-seq (**A**), or DEn enriched genes by CUT&RUN of H3K4me2 (**B**) and H3K27me3 histone marks (**C**) when comparing CM- and EM-derived HD CAR-T cells. Supplementary Fig. hows that regardless of log2 fold change (FC, x-axis) or false discovery rate (FDR, color bars) CUT&RUN identifies a larger number of unique genes differentially enriched between CM- and EM-derived CAR-T cells. False dsicovery rate (FDR) by Bonferroni correction.

Supplementary Fig. 16

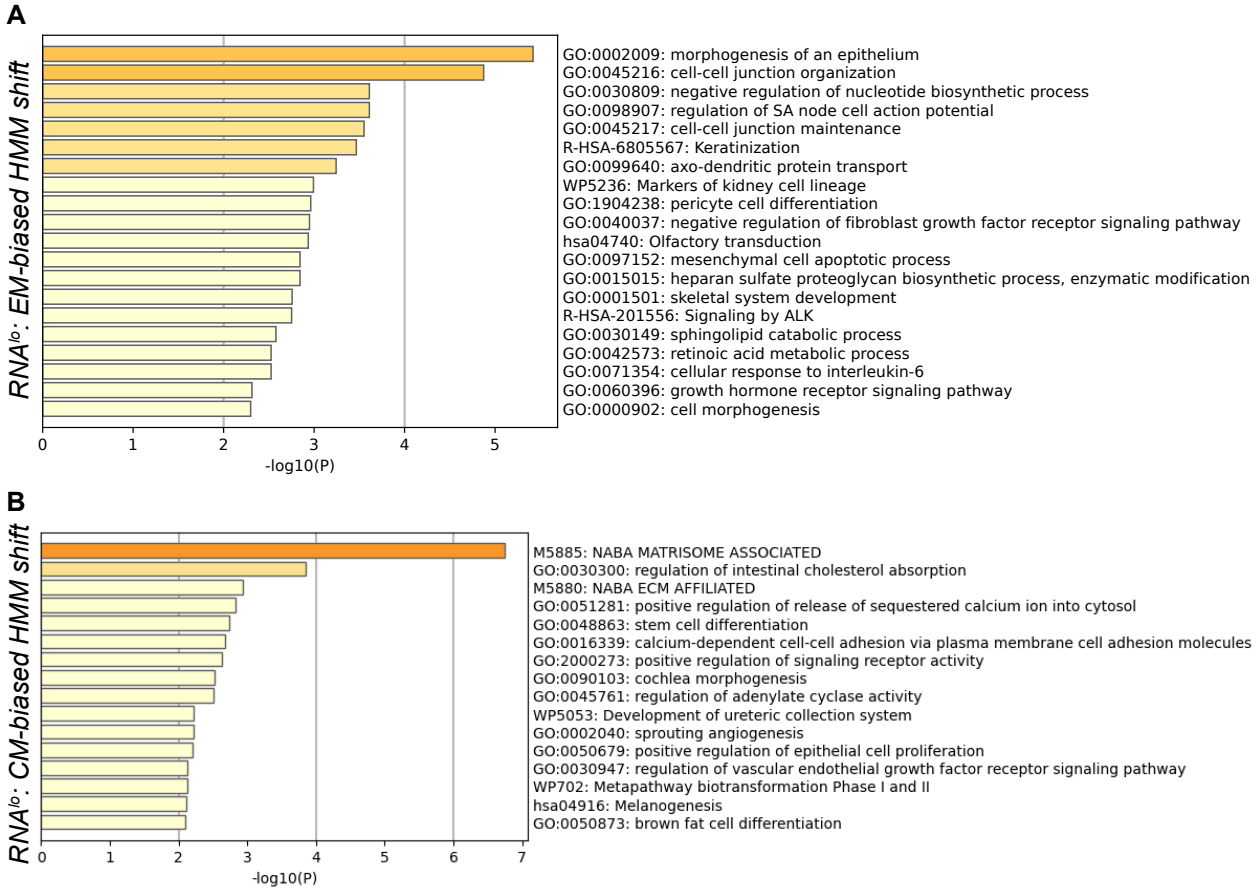

Supplementary Fig. 16. A. Gene ontology analysis by Metascape.org of RNA^{lo} genes that show histone mark patterns indicative of EM-derived CAR-T cells when compared to CM-derived CAR-T cells. **B**. Gene ontology analysis by Metascape.org of RNA^{lo} genes that show histone mark patterns indicative of CM-derived CAR-T cells when compared to EM-derived CAR-T cells. Adjusted P value by Benjamini-Hochberg procedure.

Supplementary Fig. 17

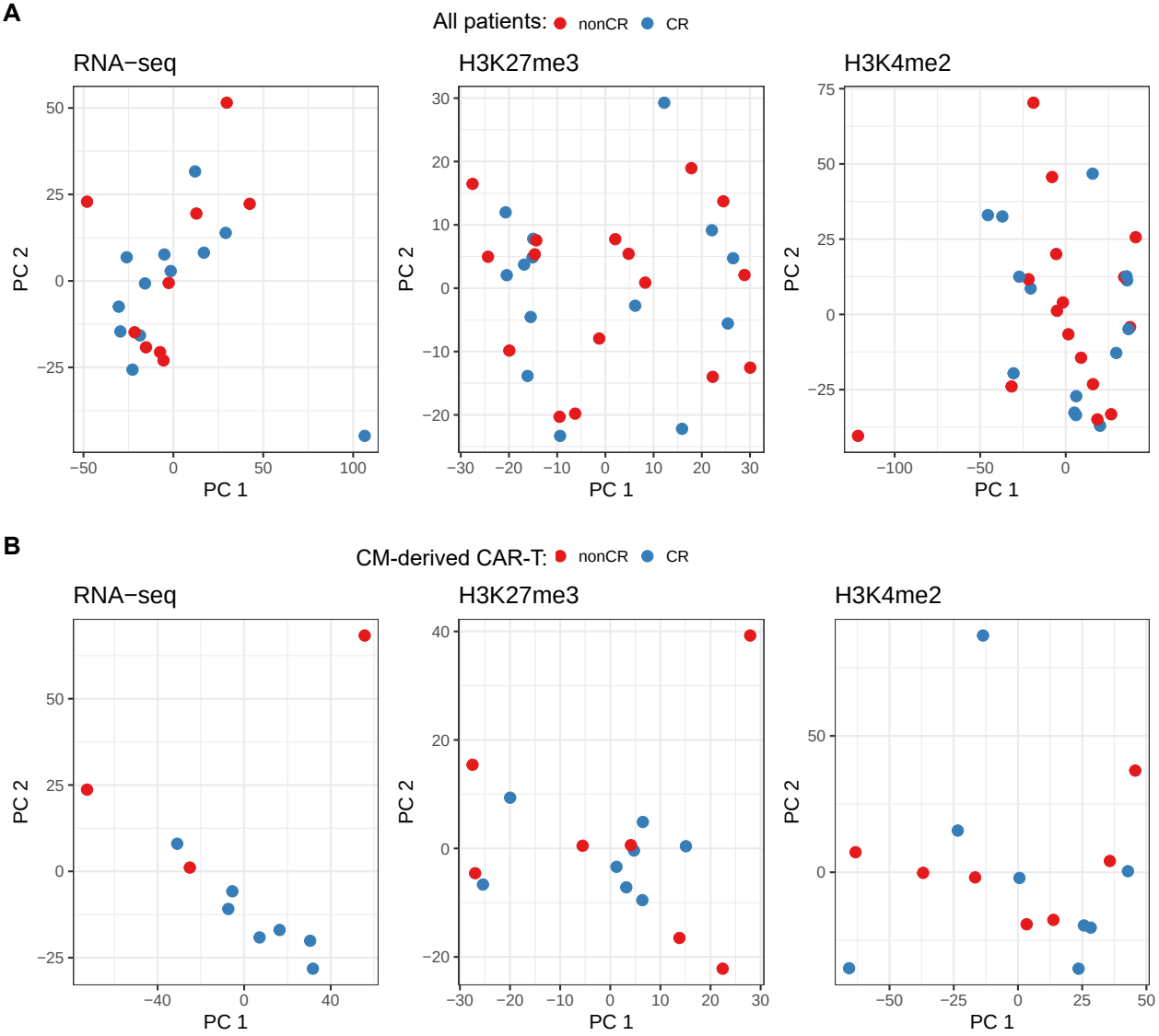

Supplementary Fig. 17. Principal component analysis plots of RNA-seq, H3K27me3 and H34me2 marks in CD8+ CAR-T cell infusion product for **A.** All patients with LBCL who showed a complete response (CR) or not (non-CR) after receiving $2x10^6$ CAR-T cells/kg in CD8:CD4 ratio of 1:1 on NCT01865617 ; **B.** Patients with LBCL who showed a complete response (CR) or not (non-CR) after receiving $2x10^6$ CAR-T cells/kg in CM-derived CD8 CAR-T cells and bulk CD4+ CAR-T cells in a ratio of 1:1 on NCT01865617.

Supplementary Fig. 18

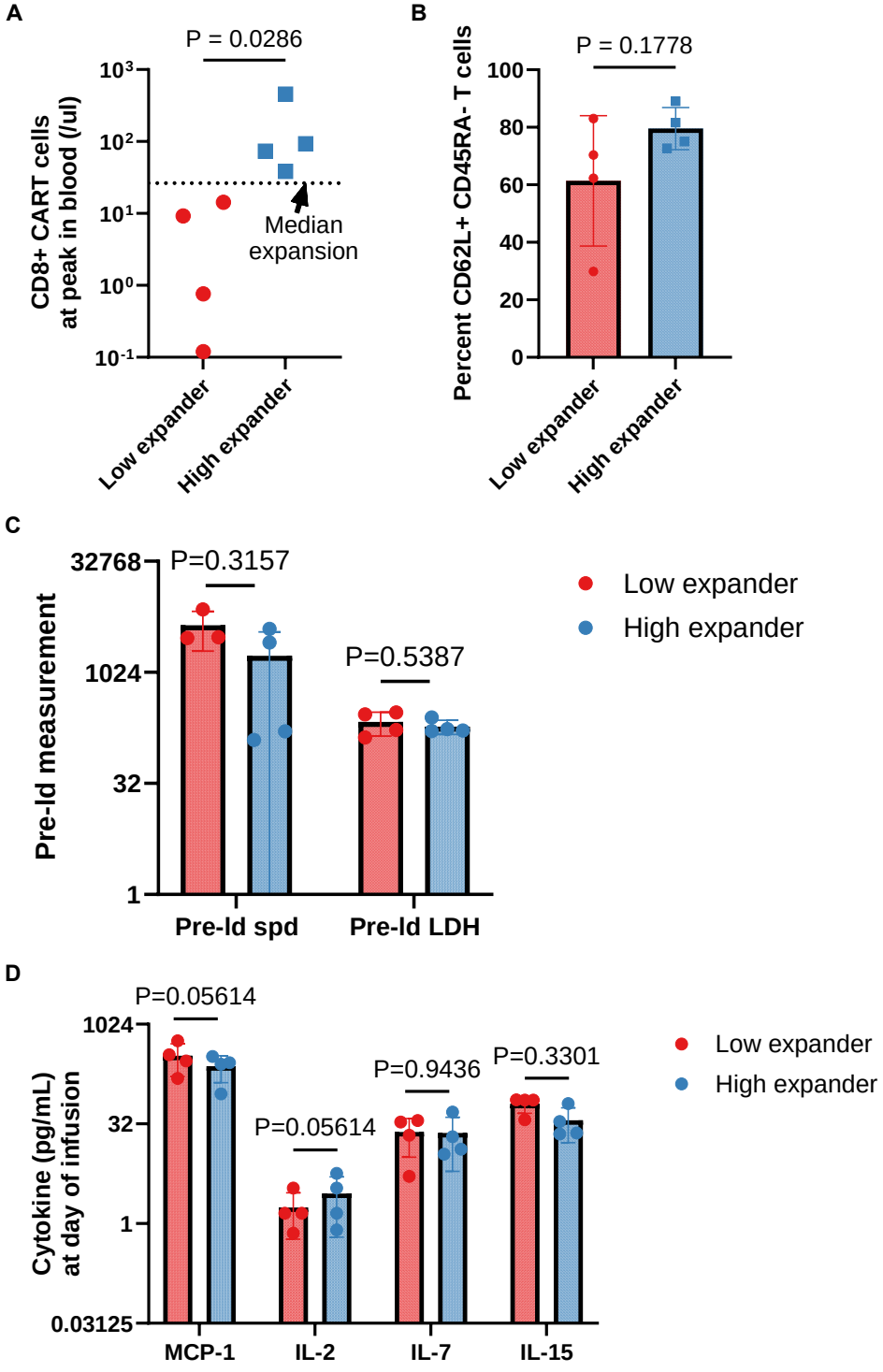

Supplementary Fig. 18. **A**. CAR-T cell numbers in peripheral blood at peak of expansion from donors used in CUT&RUN analysis with CAR-T cell count below (low expander) and above median (high expander) peak expansion. P value by Mann-Whitney test. **B**. CD62L+ and CD45RA- mean expression +/- SD on CD4-, CD45RA-depleted CD62L-selected cells prior CAR-T cell manufacture within a clinical trial (NCT01865617). P value by two-tailed t test. **C**. Pre-lymphodepletion (ld) measurement of tumor burden and activity by sum of the product of tumor diameters (spd) and lactate dehydrogenase (LDH).**D**. Serum measurements of cytokines associated with CAR-T cell proliferation and/or outcomes in previous studies at day 0 (day of CAR-T cell infusion). P value by multiple unpaired two-tailed t test with two-stage step-up.

Supplementary Fig. 19

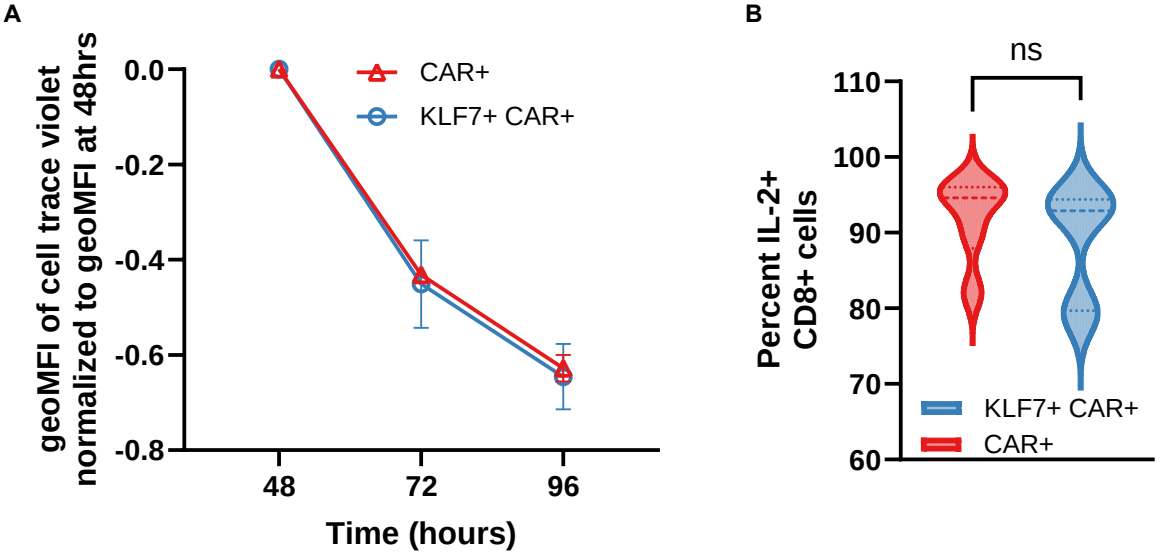

Supplementary Fig. 19. A. Mean change +/- SD in geometric mean fluorescence intensity (geoMFI) of CellTrace Violet (CTV) as an inverse measure of cell proliferation of CD19-directed CAR-T with and without KLF7 co-transduction when exposed to CD19-expressing K562 cells. n=2 donors in technical duplicate, P value by two-way ANOVA with post-hoc Tukey correction. **B**. Mean frequency and 95% confidence intervals (dotted lines) of IL-2 expressing CD19-directed CAR-T by intracellular cytokine straining with and without KLF7 co-transduction when exposed to CD19-expressing K562 cells. n=3 donors performed as technical duplicate, P value by two-tailed t test